Selected Paper

Theoretical Study on the Kinetic and Mechanism of $H + HO_2$ Reaction

Seyed Hosein Mousavipour* **and Vahid Saheb**

Department of Chemistry, College of Sciences, Shiraz University, Shiraz, Iran

Received November 21, 2006; E-mail: mousavi@susc.ac.ir

The kinetics and mechanism of reaction of a hydroperoxyl radical (HO_2) with a hydrogen atom on both singlet and triplet surfaces were studied by employing DFT, CCSD, and G3 methods along with the Aug-cc-pVTZ basis set. MC-SCF and CCD methods were used to explore potential energy surfaces. Major end products from different channels were $H_2O + O$, $H_2 + O_2$, and OH. Formation of chemically activated hydrogen peroxide HOOH was the most exothermic path in this system that dissociates to the ground state $OH(^2\Pi)$ radicals. Another energized transient species was water oxide H_2OO, which has local minimum on the singlet potential-energy surface. The energized water oxide rapidly isomerized to hydrogen peroxide HOOH or dissociated to $H_2O + O(^1D)$. Transition state theory and RRKM theory were used to calculate the rate constants for different channels.

Atomic hydrogen and hydroperoxyl radical (HO_2) are two important reactive species in many atmospheric processes and in combustion chemistry. Different sources and sinks exist for production or consumption of these two radicals in atmospheric or combustion processes. The kinetics of this system has been studied by different groups for many years.[1–19] To date, however, theoretical studies on the kinetics of this system have been hampered by the lack of an accurate mechanism. Based on the results from previous studies reported in the literature and our theoretical results, a possible mechanism for this system might be written in Scheme 1.

As shown in the above mechanism, the products are expected to be H_2, O_2, H_2O, O, and OH, as have been reported by the other researchers.[1–19] In addition, regardless of the stated electronic states, there are two paths for the formation of each product. Summary of some reported rate constants in the literature are listed in Table 1.

Early works on this system have mostly been concerned about the branching ratios of different reaction paths, formation of $H_2 + O_2$, $H_2O + O$, or 2OH. In 1972, Westenberg and DeHaas[12] have studied the decay of H atoms in a $H–O_2–M$ system. They have proposed three major paths for this system (formation of $H_2 + O_2$, $H_2O + O$, and 2OH) and determined the relative values of the rate of formation of these products to the value of disappearance rate of reactants as 0.62, 0.11, and 0.27, respectively, at 298 K.

In 1974, Baldwin et al.[13] have studied the reaction of $H + HO_2$ in a hydrogen–oxygen mixture at 773 K and over a pres-

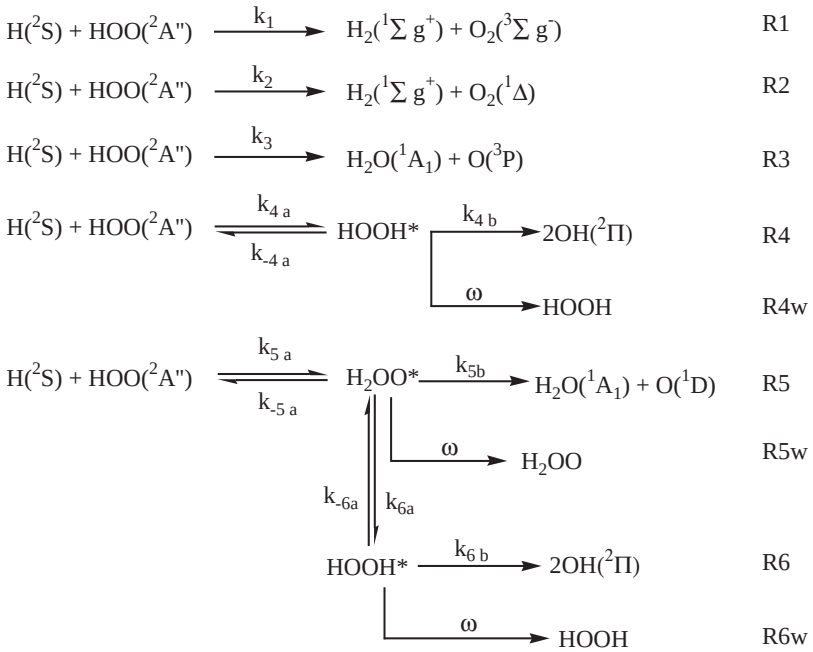

Scheme 1.

Published on the web October 12, 2007; doi:10.1246/bcsj.80.1901

Table 1. Reported Kinetic Parameters for the Reaction of Atomic Hydrogen with Hydroperoxyl Radical in the Literature[a)]

$HO_2 + H \rightarrow H_2O + O$	$HO_2 + H \rightarrow H_2 + O_2$	$HO_2 + H \rightarrow 2OH$	T/K	Ref.
1.5×10^9	3.4×10^9	4.3×10^{10}	245–300	1
$3.0 \times 10^{10} \exp(-7.2/RT)$	$4.3 \times 10^{10} \exp(-5.9/RT)$	$1.7 \times 10^{11} \exp(-3.6/RT)$	300–1000	2
		4.3×10^{11}	1160–1890	3
	$6.6 \times 10^{10} \exp(-8.9/RT)$	$1.7 \times 10^{11} \exp(-3.6/RT)$	300–2500	4
1.8×10^9	4.0×10^9	3.8×10^{10}	296	5
$5.5 \times 10^9 \exp(-7.6/RT)$	2.8×10^{10}		370–773	6
$5.0 \times 10^{10} \exp(-4.2/RT)$	$2.5 \times 10^{10} \exp(-2.9/RT)$	$2.5 \times 10^{10} \exp(-7.9/RT)$	300–1000	7
	$2.5 \times 10^{10} \exp(-2.9/RT)$	$1.5 \times 10^{11} \exp(-4.2/RT)$	300–1000	8
	$1.0 \times 10^9 \exp(1.7/RT)$	$2.8 \times 10^{10} \exp(-1.0/RT)$	231–464	9
	$1.2 \times 10^8 T^{0.75}$	$1.2 \times 10^8 T^{0.75}$	250–2000	10
		6.9×10^{10}	773	11

a) Preexponential factors are in L mol^{-1} s^{-1} and energies are in kJ mol^{-1}.

sure range of 10.5–24.8 kPa. They have reported the products were OH, $H_2 + O_2$, and $H_2O + O$ and ratio of the rate constants for the formation of OH to $H_2 + O_2$ was found as 5.9. They are not able to distinguish between reaction path for the formation of OH radicals and reaction path for the formation of $H_2O + O$. In 1979, Hack and co-workers[14] have suggested the overall rate constant for the reaction of $HO_2 + H$ as $(2.8 \pm 0.6) \times 10^{10}$ L mol^{-1} s^{-1} at 293 K and in a pressure range of 0.1 to 0.8 kPa by using a laser magnetic resonance technique. In 1981, Thrush and Wilkinson[15] have determined the total rate constant for $H + HO_2$ reaction as 3.0×10^{10} L mol^{-1} s^{-1} at 298 K and pressure range of 0.3 to 0.4 kPa using laser magnetic resonance spectroscopy method.

In 1982, Sridharan et al.[16] have measured the total rate constant for reaction $H + HO_2$ at 296 ± 2 K in a discharge-flow apparatus fitted with back-to-back laser-induced fluorescence and vacuum UV resonance fluorescence detectors. They report the rate constant for decay of the reactants as 4.5×10^{10} L mol^{-1} s^{-1} and the branching ratios for the formation of $H_2 + O_2$, $H_2O + O$, and 2OH to be 0.09 ± 0.045, 0.04 ± 0.02, and 0.87 ± 0.04, respectively. Keyser[17] has determined the total rate constant and branching ratios by using resonance fluorescence detection of radical and atomic species. The total rate constant for disappearance of the reactants is reported to be 5.2×10^{10} L mol^{-1} s^{-1} in pressure range of 0.1 to 0.3 kPa and independent of the temperature from 245 to 300 K. The resulting branching ratios are reported to be 0.08 ± 0.04, 0.02 ± 0.02, and 0.90 ± 0.04 for the formation of $H_2 + O_2$, $H_2O + O$, and 2OH, respectively.

Boutalib et al.[18] have studied the two competitive channels, reactions R1 and R3, theoretically. Saddle point geometries and barrier heights have been calculated by using SRSDCI wave functions with a valence double-zeta plus polarization basis set. The saddle points have C_S symmetry, and the barrier heights for reactions R1 and R3 are reported as 22.2 and 82.8 kJ mol^{-1}, respectively. They have used transition-state theory to calculate the kinetic parameters. They report the Arrhenius parameters for reactions R1 and R3 for temperatures close to 300 K: $k_1 = 2.0 \times 10^{10}$ L mol^{-1} s^{-1} $\exp(-9.7$ kJ mol$^{-1}/RT)$ and $k_3 = 2.0 \times 10^{10}$ L mol^{-1} s^{-1} $\exp(-83.8$ kJ mol$^{-1}/RT)$. Their results show that hydrogen abstraction from HO_2 is more plausible than disproportionation reaction R3.

A theoretical study has been reported by Karkach and Osherov[19] at the QCISD(T)/6-311(d,p) level on the lowest triplet potential energy surface for the dissociation of H_2O_2. They have not considered the other possible reaction paths on singlet surfaces. They have studied the kinetics of different channels in that system and report values of 7.5 and 60.8 kJ mol^{-1} for the barrier heights of reactions R1 and R3, respectively.

According to the above mechanism, molecular and atomic oxygen might be produced on both triplet or singlet surfaces (reactions R1 and R2 for the formation of O_2 and reactions R3 and R5 for the formation of atomic oxygen). Also, two different channels are suggested for the formation of hydroxyl radicals (reactions R4 and R6).

One major discrepancy between the experimental studies and theoretical studies is the reported Arrhenius expressions for the formation of $H_2O + O$. As indicated in Table 1, all experimental studies report activation energy values of zero to 7.6 kJ mol^{-1} for the formation of $H_2O + O$, whereas in the theoretical works (Refs. 18 and 19) values of 82.8 and 60.8 kJ mol^{-1} are reported for the activation energy of reaction R3. In the present study, we attempted to answer the possible reasons for these discrepancies.

One interesting aspect in this system is the presence of transient species water oxide, H_2OO. Some researchers reported the possibility of existing water oxide as a short-lived species in gas phase and also in liquid phase, which undergoes isomerization process according to reaction R6a or dissociates to $H_2O + O$ according to reaction R5b.[20]

It has been proposed by Schröder et al.[20f] that water oxide can be formed as a transient species on the singlet potential energy surface in the $H_2 + O_2$ system. To the best of our knowledge, their work is the first experimental report on the existence of water oxide. According to their results, singlet water oxide is 196.5 kJ mol^{-1} less stable than hydrogen peroxide. Sayos et al.,[20i] in a quasiclassical trajectory study on the reaction of $O(^1D) + H_2O(^1A_1)$, have shown that water oxide is 211.9 kJ mol^{-1} less stable than hydrogen peroxide at UMP2 level of theory. Filatov et al.[20j] have studied the reason for the kinetic stability of the $H_2 + O_2$ mixture. They have reported that water oxide is 209.4 kJ mol^{-1} less stable than hydrogen peroxide at the MR-(S)DCI/cc-pVTZ level.

Toohey and Anderson,[21] in a theoretical study on the reaction of some small radicals with HO_2, have considered a transition structure of HHOO species with an imaginary frequency and a barrier height of 23.0 kJ mol^{-1} relative to the total energy of $H + HO_2$ at the UMP2/6-31G** level. It seems that they have only considered the structure of H–H–O=O instead of considering the structure of water oxide. This energized intermediate has been reported to exist with a short lifetime which dissociates to $H_2O + O(^1D)$ according to channel R5 or undergoes isomerization to produce energized HOOH*, which then dissociates to $OH(^2\Pi)$ via channel R6 or undergoes stabilization process according to R6w. The produced energized hydrogen peroxide in channel R6 undergoes dissociation process to produce hydroxyl radicals unless stabilizes under collision with the other species.

It was the aim of this study to investigate the singlet and triplet potential energy surfaces of different channels in this system and also to verify theoretically the contribution of each step to the formation of possible products in the proposed mechanism. As shown in the above mechanism, two channels are suggested for the formation of $H_2O + O$ and two channels for the formation of OH radicals. We also characterized the effect of chemically activation processes involved in channels R5 and R6.

Generalized transition state theory and RRKM method were used to calculate the rate constants. To calculate the rate constant for reaction R4 that proceeds via chemically activation process, a RRKM-TST model from Berman and Lin[22] was used. Reactions R5 and R6 proceed via chemically activation process, in which two energized species water oxide H_2OO* and hydrogen peroxide HOOH* are formed and undergo stabilization or dissociation process simultaneously. To calculate the overall rate constants for channels R5 and R6, a method based on RRKM theory introduced by Dean was used.[23]

Ab Initio Calculations

All ab initio calculations were carried out using the Gaussian03 program suite.[24] Geometric parameters of the relevant stationary points were optimized at the MP2,[25] B3LYP,[26] KMLYP,[27] CAS(MP2),[28] CCSD,[29] and G3[30] levels of theory in conjunction with augmented correlation-consistent basis set Aug-cc-pVTZ.[31] The potential energy surfaces were explored at the UMP2, B3LYP, CAS(6,6), and CCD(T) levels using 6-311+G(2d,2p) basis set. Harmonic vibration frequencies were obtained at the CCD/6-311+G(2d,2p) level in order to characterize the stationary points as local minima or first-order saddle points, to obtain zero-point vibration energy corrections, and to generate force constant data needed in the intrinsic reaction coordinate (IRC)[32] calculations for those channels with a saddle point. The IRC method was used to track minimum energy paths (MEP) from transition structures to the corresponding local minima. The projected frequencies were computed for vibrations perpendicular to the path along the IRC for those reactions with no saddle point. The calculated term values were scaled by 0.94.

The enthalpies of different reaction paths at 298 K were calculated at the G3 level and compared with the reported values in the literature in Table 2.

Table 2. The Enthalpies of Reactions $\Delta_r H^0$ Calculated at the G3 Level in kJ mol^{-1}

Reaction	G3	$\Delta_r H^0{}_{exp}$ [a)]
$H + HO_2 \rightarrow H_2O + O$	−223.3	−221 ± 3
$H + HO_2 \rightarrow H_2 + O_2$	−228.8	−228 ± 3
$H + HO_2 \rightarrow HOOH$	−362.6	−364 ± 3
$HOOH \rightarrow 2OH$	201.4	211 ± 3
$H + HO_2 \rightarrow 2OH$	−161.2	−153.3 ± 1 −161[b)]
$H + HO_2 \rightarrow H_2OO$	−169.3	
$H_2OO \rightarrow HOOH$	−193.3	

a) From experimental standard heats of formations from Refs. 33, 34, and 35. b) From Ref. 36.

Energies and Geometries

Figure 1 shows the optimized geometries of all stationary points. Figure 2 shows the relative energies of different species at the CCSD(full)/Aug-cc-pVTZ and G3 levels. These values were corrected for ZPEs. In Table 3, total energies of all stationary points at different levels of theory and zero point energies calculated at the CCD/6-311+G(2d,2p) level are listed. The corrected barrier heights for ZPEs are shown in Table 4. Vibrational term values and rotational constants are listed in Table 5. In this study, the vibrational term values and moments of inertia for HO_2 from Refs. 37 and 38, and for H_2O and H_2O_2 from Refs. 39, 40, and 41, and for H_2, O_2, and OH from Ref. 42 were used, respectively.

Transition State Theory

Generalized transition state theory was used to calculate the rate constants for reactions R1, R2, and R3 that proceed via saddle point:[43]

$$k(T,s) = \Gamma \frac{k_B T}{h} \sigma \frac{Q^{\ddagger}(T,s)}{Q_A Q_B(T)} \exp\left(\frac{-V_{MEP}(s)}{k_B T}\right), \quad (1)$$

where Γ is the tunneling factor,[44] k_B and h are Boltzmann's and Planck's constants, T is the temperature, σ is the reaction path degeneracy (the ratio of symmetry numbers from the rotational partition functions), Qs represent the products of rotational, vibrational, and translational partition functions for the transition state (numerator) and reactants (denominator), s is the distance along the reaction path, and V_{MEP} is the potential energy corrected for zero-point energy at the generalized transition-state locations at zero degree.

The tunneling correction factor is defined as the quotient of the quantum mechanical rate to the classical rate.[45] In the case of a symmetrical Eckart barrier,[46] a simple expression for the tunneling correction is suggested by Shavitt:[47]

$$Q_{tunnel} = 1 - \frac{1}{24}\left(\frac{h\nu^*}{k_B T}\right)^2 \left(1 + \frac{k_B T}{E_0}\right), \quad (2)$$

where ν^* is the imaginary frequency of the activated complex at the top of the barrier, k_B and h are Boltzmann's and Plank's constants, respectively, and E_0 is the barrier height corrected for zero point energy for the reaction. In another method to calculate the tunneling factor, it is assumed a particle with energy of E approaching an unsymmetrical Eckart barrier. In this method the tunneling factor can be calculated as[48]

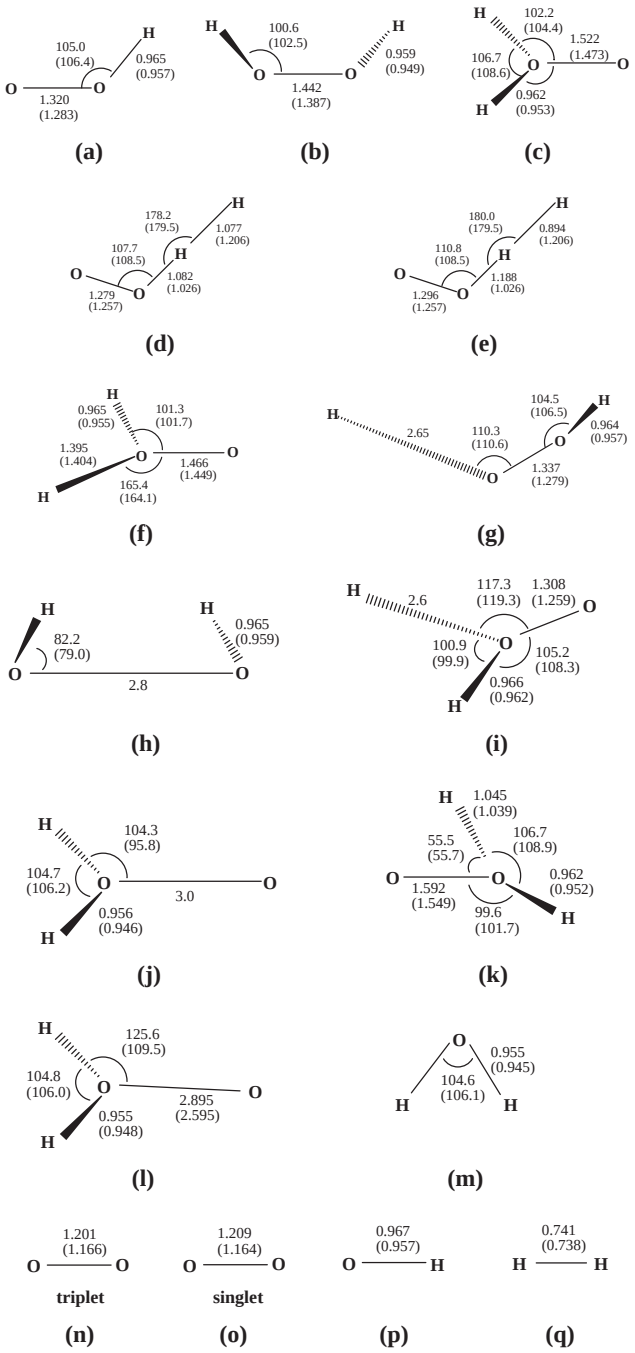

Fig. 1. Optimized geometries of HO_2 (a), HOOH (b), ^1H_2OO (c), transition state of reactions R1 (d), R2 (e), R3 (f), R4a (g), R4b (h), R5a (i), R5b (j), and R6a (k), ^3H_2OO (l), H_2O (m), $^3O_2$ (n), $^1O_2$ (o), OH (p), and H_2 (q), respectively, at the CCSD/Aug-cc-pVTZ level. Values in the parentheses are from KMLYP/Aug-cc-pVTZ optimization.

$$\Gamma = \exp(V/k_BT)\int_0^\infty \kappa(E)\exp(-E/k_BT)\mathrm{d}E/k_BT, \qquad (3)$$

where V is the effective barrier height corrected for zero point energy, and $\kappa(E)$ is the transmission probability for a particle with the energy E approaching an Eckart barrier. To calculate the tunneling factor, a numerical integration program of

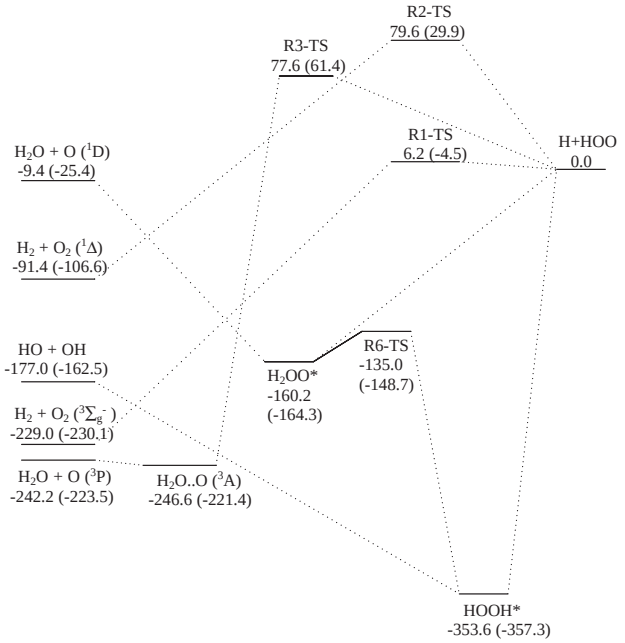

Fig. 2. Relative energies of different species in kJ mol^{-1} at the CCSD(full)/Aug-cc-pVTZ level (numbers in parentheses are from G3 calculations). All values are corrected for zero point energies.

Brown[49] was used. Γ in Eq. 3 is related to the barrier heights for forward and reverse reaction and frequency of an imaginary vibration, ν^*, in a well created by inverting the barrier. To calculate the value of Γ according to Eq. 3, α_i ($=2\pi V_i/h\nu^*$ where i is 1 or 2 for forward or reverse reaction, respectively) and u^* ($=h\nu^*/k_BT$) were introduced to the program as input.

Rate Constants for Reactions R1, R2, and R3

Figure 3 shows the vibrationally adiabatic ground state potential energy surfaces for the formation of $H_2(^1\Sigma_g^+) + O_2(^3\Sigma_g^-)$ on the triplet and $H_2(^1\Sigma_g^+) + O_2(^1\Delta)$ on the singlet surfaces (reactions R1 and R2) and formation of $H_2O(^1A_1) + O(^3P)$ over the triplet surface, reaction R3, at CCD/6-311+G(2d,2p) level. As shown in Fig. 2 and listed in Tables 3 and 4, the triplet surface was more favorable than the singlet surface for the formation of $H_2 + O_2$ at different levels of theory. Washida and co-workers,[36] in a kinetic study of $H + O_2$ system have reported the probability for reaction R1 is 40 times more than that for reaction R2. Boutalib and co-workers[18] have reported a value of 22.1 kJ mol^{-1} for the barrier of reaction R1, whereas Michael et al.[50] have reported values of 10.9 to 12.1 kJ mol^{-1} for the barrier of this reaction at the CCSD(T) level using different basis sets. Karkach and Osherov[19] have reported a value of 7.5 kJ mol^{-1} for the barrier of this channel. Our results for the barrier height of this channel from different levels of theory are listed in Table 4. We estimated a value of 6.2 kJ mol^{-1} for the barrier height of reaction R1 from CCSD(full)/Aug-cc-pVTZ calculations.

As shown in Fig. 2, a short-lived species ^3H_2OO formed along the triplet surface towards the formation of $H_2O(^1A_1) + O(^3P)$.[20f] Its total energy was only 4.4 kJ mol^{-1} less than the

Table 3. Calculated Total Energies of All Species in Atomic Unit at Different Levels of Theory Along with the Aug-cc-pvTZ Basis Set[a)]

Species	MP2	MP4(SDQ)	KMLYP	B3LYP	CCSD=full	CCSD(T)	CAS(6,6)MP2	G3	ZPE
$H(^2S)$	−0.49982	−0.49982	−0.52022	−0.50226	−0.49982	−0.49982		−0.50100	
$O(^1D)$	−74.86546	−74.88766	−75.02987	−74.99311	−74.89818	−74.89795		−74.95554	
$O(^3P)$	−74.97077	−74.98639	−75.13394	−75.09418	−74.98682	−74.97895		−75.03099	
$H_2(^1\Sigma_g^+)$	−1.16501	−1.17202	−1.22290	−1.18002	−1.17263	−1.17263		−1.16737	0.01008
$OH(^2\Pi)$	−75.63985	−75.65273	−75.82971	−75.76854	−75.65309	−75.64555		−75.69491	0.00866
O_2 $(^3\Sigma_g^-)$	−150.14846	−150.15155	−150.44887	−150.38459	−150.14997	−150.14083		−150.24820	0.00382
O_2 $(^1\Delta)$	−150.10122	−150.09992	−150.38315	−150.32334	−150.09740	−150.09327		−150.20114	0.00367
$H_2O(^1A_1)$	−76.34412	−76.34924	−76.55336	−76.46609	−76.34876	−76.34224		−76.38204	0.02188
HOO $(^2A'')$	−150.72115	−150.73453	−151.06481	−150.97317	−150.73636	−150.72639		−150.82691	0.01472
H_2OO	−151.29673	−151.31023	−151.66371	−151.54570	−151.30984	−151.30106	−150.86751	−151.39047	0.02735
HOOH	−151.37738	−151.38471	−151.73771	−151.61778	−151.38347	−151.37402	−150.94158	−151.46415	0.02734
H + HOO	−151.22097	−151.23435	−151.58503	−151.47543	−151.23618	−151.22621	−150.80635	−151.32791	0.01472
HO + OH	−151.27970	−151.30546	−151.65942	−151.53708	−151.30618	−151.29110	−150.87970	−151.38982	0.01732
$H_2O + O(^1D)$	−151.20958	−151.23690	−151.58323	−151.45920	−151.24694	−151.24019	−150.80548	−151.33758	0.02188
$H_2O + O(^3A)$	−151.28971	−151.31070	−151.68890	−151.56161	−151.33737	−151.32282		−151.41224	0.02197
TS1	−151.21154	−151.22684	−151.58416	−151.48652	−151.23151	−151.22414		−151.32963	0.01243
TS2	−151.21431	−151.20987	−151.53843	−151.45622	−151.20692	−151.21072		−151.31651	0.01578
TS3	−151.17746	−151.20060	−151.55704	−151.45711	−151.20892	−151.20166		−151.30452	0.01702
TS6a	−151.28597	−151.29634	−151.64427	−151.53368	−151.29561	−151.29065		−151.38454	0.02274

a) Zero point energies (ZPE) are calculated at the CCD/6-311+G(2d,2p) level.

Table 4. Corrected Barrier Heights for Zero Point Energies for Different Paths in kJ mol^{-1}

Method of Calc.	R1	R2	R3	R-4a	R4b	R-5a	R5b	R6a	R-6a
MP2/AUG-CC-PVTZ	18.7	20.3	120.3	377.5	230.2	165.7	214.5	16.1	227.9
MP4(SDQ)/AUG-CC-PVTZ	13.7	67.1	94.6	361.6	181.8	166.1	178.2	24.4	219.9
B3LYP/AUG-CC-PVTZ	−35.1	53.2	54.1	340.6	185.6	151.3	212.7	19.4	208.7
CCSD=full/AUG-CC-PVTZ	6.2	79.6	77.6	353.6	176.6	160.2	150.8	25.2	218.6
CCSD(T)/AUG-CC-PVTZ	−0.6	76.1	70.5	354.9	191.4	163.4	145.4	15.2	206.8
CAS(6,6)MP2/AUG-CC-PVTZ				321.9	136.1	127.4	148.5		
SVWN/AUG-CC-PVTZ	−3.8	125.1	79.5	367.7	179.2	173.4	196.9	38.9	233.2
G3	−4.5	29.9	61.4	357.7	195.1	164.2	138.9	15.6	209.0

Table 5. Vibrational Frequencies and Moments of Inertia for Different Species in H + HO_2 System Calculated at the CCD/6-311+G(2d,2p) Level of Theory

Species	I_i/au	Frequencies/cm^{-1}
HO–O	0.80, 14.79, 15.59	3552.8, 1415.5, 1123.7
H_2O–O	1.70, 20.84, 21.54	3683.3, 3596.2, 1578.8, 889.8, 888.1, 684.3
HOOH	1.64, 18.88, 19.50	3657.2, 3656.1, 1403.2, 1301.0, 916.0, 384.3
TS1	4.06, 16.52, 20.58	1466.0, 1349.1, 1215.2, 742.3, 370.8, 2679.6i
TS2	2.59, 16.79, 18.70	2312.9, 1482.5, 1291.4, 764.0, 682.5, 1755.4i
TS3	1.02, 22.15, 23.16	3602.3, 1348.5, 1038.9, 572.5, 481.1, 2204.2i
TS4a	5.65, 19.73, 23.76	3580.2, 1408.5, 1171.3, 407.4, 313.8
TS4b	1.75, 66.12, 67.69	3673.8, 3620.8, 459.9, 435.2, 117.0
TS5a	4.88, 19.81, 23.09	3578.6, 1505.9, 1419.4, 373.9, 275.6
TS5b	1.65, 78.23, 78.88	3772.2, 3677.0, 1594.1, 155.6, 146.2
TS6a	1.58, 21.79, 22.24	3711.9, 2811.2, 1365.0, 995.6, 696.7, 1517.8i

total energy of $H_2O(^1A_1)$ + $O(^3P)$, and it turned out to be unstable towards dissociation into $H_2O(^1A_1)$ + $O(^3P)$. Therefore, in our rate constant calculations, we ignored the role of this species, which is highly vibrationally excited. Boutalib and co-workers[18] have reported a value of 82.8 kJ mol^{-1} for the barrier of reaction R3, whereas Karkach et al. have reported a value of 60.8 kJ mol^{-1} for the barrier of this channel. We calculated the barrier height for this channel at different levels of theory, and the values are listed in Table 4. To calculate the rate constant for reaction R3, we used a value of 77.6 kJ mol^{-1} for the barrier height of this channel from CCSD(full) results. To the best of our knowledge, no specific kinetic data is available for channel R2 (formation of H_2 + O_2 $(^1\Delta)$), to which we could compare our results.

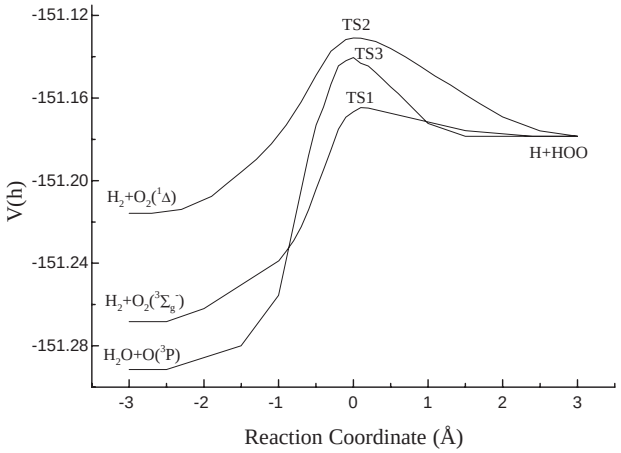

Fig. 3. The Born–Oppenheimer potential energies (V_{MEP}) and the vibrationally adiabatic ground state potential energy surfaces along the reaction paths R1, R2, and R3 computed at the CCD(full)/6-311+G(2d,2p) level.

Equation 1 was used to calculate the rate constants for reactions R1, R2, and R3 using the data from Tables 4 and 5. Equation 3 was used to calculate the tunneling corrections for reactions R1, R2, and R3.[49]

Figures 4 and 5 show the Arrhenius plots for reactions R1, R2, and R3. In Figs. 4 and 5, we compared our results with the reported rate constants for $H_2 + O_2$ and $H_2O + O$ formation in the literature. In Fig. 4a, we compared our calculated values of k_1 from CCSD(full) results (solid line) and from CCSD(T) results (dashed-dot-dot line) with the previous rate constants reported for $H_2 + O_2$ formation. In Fig. 4b, we compared our calculated values for k_2 with the data in Fig. 4a for k_1. The agreement between our calculated k_1 with the experimental results in the literature indicates that the main path for the formation of $H_2 + O_2$ is channel R1 that proceeds over a triplet surface. To the best our knowledge, no electronic state for produced O_2 is reported in the previous experimental studies. Washida et al.[36] have studied the electronic state of produced O_2 in this system, but they do not report the individual relevant rate constants. The calculated rate constant for reaction R2 at different levels of theory is much smaller than the values for k_1. The rate constant expressions for k_1 from CCSD(full) and CCSD(T) calculations were found to be $k_1 = 6.7 \times 10^4 \times T^{1.77} \times \exp(+2.38\,\mathrm{kJ\,mol^{-1}}/RT)\,\mathrm{L\,mol^{-1}\,s^{-1}}$ from CCSD(full) results and $k_1 = 1.86 \times 10^5 \times T^{1.72} \times \exp(+4.84\,\mathrm{kJ\,mol^{-1}}/RT)\,\mathrm{L\,mol^{-1}\,s^{-1}}$ from CCSD(T) results. The rate constant expressions for k_2 from CCSD(full) and G3 calculations were found to be $k_2 = 1.61 \times 10^4 \times T^{1.63} \times \exp(-63.94\,\mathrm{kJ\,mol^{-1}}/RT)\,\mathrm{L\,mol^{-1}\,s^{-1}}$ from CCSD(full) results and $k_2 = 1.65 \times 10^5 \times T^{1.63} \times \exp(-16.87\,\mathrm{kJ\,mol^{-1}}/RT)\,\mathrm{L\,mol^{-1}\,s^{-1}}$ from G3 results.

Figure 5 shows the Arrhenius plot for channel R3. In Fig. 5, we compared our calculated values for k_5 at different levels of theory with the reported values for the rate constant of reaction R3 reported by Boutalib et al.[18] and Karkach and Osherov.[19] As shown in Fig. 5 our results at the CCSD(full)/Aug-cc-pVTZ level is in better agreement with the previous results. The rate constant expressions for reaction R3 calculated at different levels of theory were found to be $k_3 = 9.1 \times 10^5 \times T^{1.47} \times \exp(-58.1\,\mathrm{kJ\,mol^{-1}}/RT)\,\mathrm{L\,mol^{-1}\,s^{-1}}$ from CCSD(T) results and $k_3 = 3.3 \times 10^5 \times T^{1.58} \times \exp(-68.2\,\mathrm{kJ\,mol^{-1}}/RT)\,\mathrm{L\,mol^{-1}\,s^{-1}}$ from CCSD(full) results and $k_3 = 8.6 \times 10^5 \times T^{1.48} \times \exp(-50.6\,\mathrm{kJ\,mol^{-1}}/RT)\,\mathrm{L\,mol^{-1}\,s^{-1}}$ from G3 results.

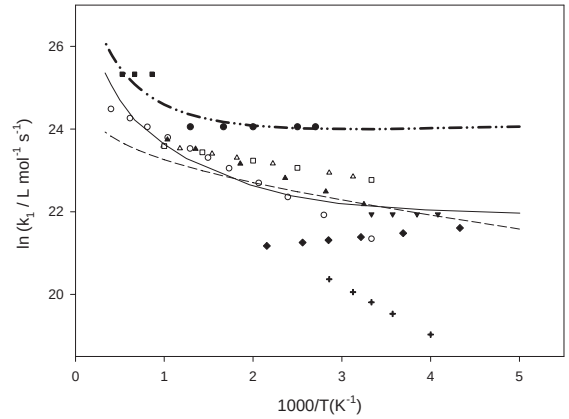

(a)

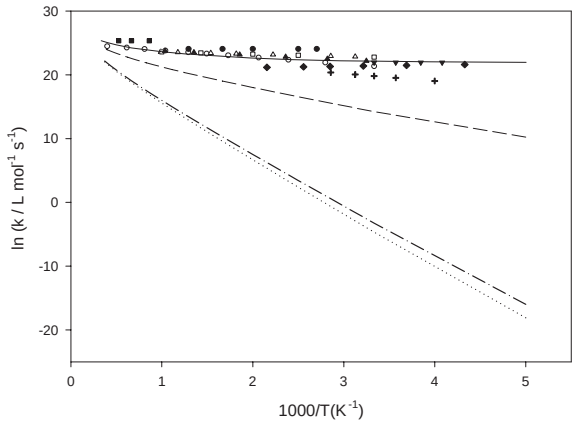

(b)

Fig. 4. (a) Arrhenius plot for reaction R1: solid line is calculated from CCSD(full) results, dashed-dot-dot line from CCSD(T) results, dashed line from Ref. 19, (+) from Ref. 18, (▼) from Ref. 1, (■) from Ref. 3, (▲) from Ref. 2, (○) from Ref. 4, (△) from Ref. 8, (●) from Ref. 6, (□) from Ref. 7, (◆) from Ref. 9. (b) Arrhenius plot for reaction R2 is compared with the data in (a), long-dashed line from G3 results, dashed-dot line from CCSD(T) results, and dotted line from CCSD (full) results, solid line and the symbols are as described in (a).

Rate Constant for Channel R4

Reaction R4 proceeds through the formation of chemically activated molecule HOOH*, see Fig. 2. In reaction R4, the total energy of the chemically activated hydrogen peroxide was 353.6, 354.6, and 357.3 kJ mol^{-1} lower than the total energies of the reactants at the CCSD(full), CCSD(T), and G3 levels, respectively, at zero Kelvin. This amount of energy release into the newly formed molecule HOOH* causes this molecule to undergo dissociation process unless stabilizes under collision with the other species, reaction R4w. As shown in Fig. 6, no saddle points were observed for the formation

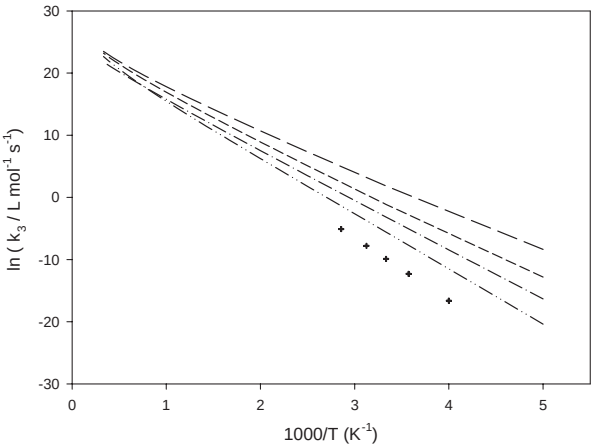

Fig. 5. Arrhenius plot for reaction R3 at different levels of theory. Long-dashed line from G3 results, short-dashed line from CCSD(T) results, dashed-dot-dot line from CCSD(full) results and dashed-dot line from Ref. 19, + from Ref. 18.

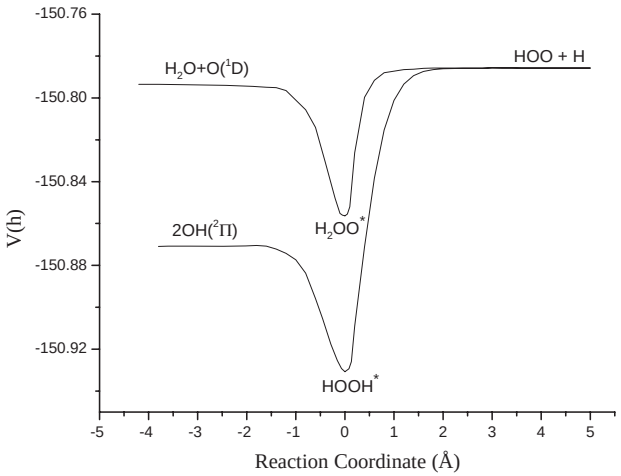

Fig. 6. Born–Oppenheimer potential energies (V_{MEP}) and the vibrationally adiabatic ground state potential energy surfaces for reactions R4 and R5 computed at the CAS(6,6)/6-311+G(2d,2p) level.

or dissociation of hydrogen peroxide at the CAS/6-311+G(2d,2p) level. The potential energy surface for dissociation of hydrogen peroxide has been studied by several groups, theoretically and experimentally, for example, see Ref. 51 and references therein. To calculate the rate constant for reaction R4, we first searched for the location of the bottlenecks for the entrance and exit channels of formation of energized molecule HOOH*. Microcanonical variational RRKM calculations were performed to locate the position of the bottlenecks. Figure 6 was used to calculate the sum and density of states of the system at different H–O or O–O bond lengths for the entrance or exit channels of HOOH, respectively. A standard RRKM program by Zhu and Hase[52] was used to calculate the sum and density of states. The following expression is normally used to calculate the unimolecular rate constant as a function of pressure.[53]

$$k_{\mathrm{uni}} = \frac{\sigma B_{\mathrm{e}}}{hQ_{\mathrm{r}}} \times \exp\left(\frac{-E_0}{RT}\right)\Delta E^{+}\sum_{J=0}^{\infty}\left[\frac{(2J+1)\{G(E^{+}_{\mathrm{vr}})\}\exp\left(\frac{-E^{+}}{RT}\right)}{1+\frac{k(E)}{\omega}}\right], \quad (4)$$

where σ is the statistical factor (the reaction path degeneracy), B_{e} is the ratio of electronic partition functions, Q_{r} represents the product of partition functions for the reactant, E_0 is the potential energy barrier which corrected for zero-point energy, E^{+} is the total non-fixed energy of a given transition state, ΔE^{+} is the energy increment. $G(E^{+}_{\mathrm{vr}})$ is the sum of vibrational–rotational states of the transition state, $k(E)[=G(E^{+})/hN(E_{\mathrm{v}})]$ is the rate constant for conversion of energized molecule to products, $N(E_{\mathrm{v}})$ is density of states, and ω ($=Z\beta_{\mathrm{c}}[A]$) is the collisional stabilization rate constant, of which β_{c} is the collision efficiency. To locate the position of bottleneck, the RRKM program searches for the minimum in the sum of states versus reaction coordinate as a function of available energy (temperature).[54] Rabinovitch and Whitten[55] have suggested only a fraction of the zero-point energy (aE_{z}) should be included in the classical energy at each point along the reaction coordinate and have recommended the following expression to calculate the sum of state:

$$G(E^{+}) = \frac{(E^{+}+aE_{\mathrm{z}})}{s!\prod_{i=1}^{s}h\nu_i} \quad (5)$$

In RRKM calculations, a step size of $\Delta E^{+} = 0.4\,\mathrm{kJ\,mol^{-1}}$ up to $E^{+} = 10\,\mathrm{kJ\,mol^{-1}}$ at 200 K, which was increased to a value of $100\,\mathrm{kJ\,mol^{-1}}$ at 3000 K, was used. In these calculations the external rotations were treated as being adiabatic. B_{e} was assumed to be equal 1. N_2 was chosen as bath gas and a value of 0.2 was selected for the collision efficiency β_{c} from Ref. 56. We noticed that two vibrational frequencies were changing significantly along the reaction coordinates for dissociation of hydrogen peroxide towards the reactants ($H + HO_2$) or product (2OH). The results of microcanonical variational RRKM calculations for reactions R4a and R4b are summarized in Tables 6 and 7, respectively.

After locating the position of the bottlenecks for reactions R4a and R4b, a RRKM-TST model from Berman and Lin[22] was used to calculate the rate of disappearance of the reactants according to the mechanism shown for channel R4. According to this method and based on the proposed mechanism for channel R4, the bimolecular rate constant can be calculated according to Eq. 6.

$$k_{\mathrm{bi}} = \frac{\sigma B_{\mathrm{e}}}{hQ_{\mathrm{r}}} \times \exp\left(\frac{-Ea}{RT}\right)\int_{0}^{\infty}\frac{(\omega+k_{\mathrm{e}})\{G(E^{+}_{\mathrm{vr}})\}\exp\left(\frac{-E^{+}}{RT}\right)}{(w+k_{\mathrm{e}}+k'_{\mathrm{e}})}\mathrm{d}E^{+} \quad (6)$$

Here, the bimolecular rate constant k_{bi} is expressed as a function of reaction probabilities k_{e} and k_{e}' for the dissociation of energized adducts (shown as $k_{4\mathrm{b}}$ and $k_{-4\mathrm{a}}$ in reaction R4,

Table 6. Microcanonical Variational RRKM Results for Unimolecular Dissociation Step R4a

$E(v,j)$[a]	$E^{\#}(v,j)$[b]	$R^{\#}/\text{Å}$[c]	E_0[d]	$N(v,j)$[e]	$G(E^{\#})$[f]	$k(E) \times 10^{11}(1/s)$
355.6	11.0	2.85	375.6	19.5	4	0.06
366.1	21.8	2.76	374.1	22.0	15	0.20
376.6	32.8	2.69	373.8	24.7	37	0.45
387.0	43.6	2.64	373.5	27.7	77	0.83
397.5	54.5	2.60	373.0	31.1	145	1.40
407.9	65.5	2.56	372.2	34.7	252	2.18
418.4	76.6	2.52	371.9	38.6	410	3.18
428.9	87.8	2.48	370.3	42.9	635	4.43
439.3	98.6	2.45	370.1	47.6	935	5.88
449.8	109.5	2.43	370.0	52.7	1348	7.68
460.2	120.5	2.41	368.8	58.1	1893	9.76
470.7	131.5	2.39	368.7	64.1	2595	12.14
481.2	142.6	2.37	368.1	70.5	3486	14.82
491.6	153.8	2.35	366.6	77.4	4598	17.81
502.1	165.1	2.33	365.5	84.9	5969	21.09
512.5	176.3	2.31	365.0	92.9	7639	24.66
523.0	187.7	2.29	364.9	101.5	9652	28.51
533.5	199.1	2.27	363.4	110.7	12050	32.64
543.9	209.7	2.25	362.0	120.6	14760	36.71

a) The total energy available to the system in kJ mol^{-1}. b) The transition-state energy in kJ mol^{-1}. c) The position of bottle-neck in angstrom. d) The classical energy difference between the reactant and the transition state in kJ mol^{-1}. e) The density of states in cm^{-1}. f) The sum of states.

Table 7. Microcanonical Variational RRKM Results for the Unimolecular Dissociation Step R4b

$E(v,j)$[a]	$E^{\#}(v,j)$[b]	$R^{\#}/\text{Å}$[c]	E_0[d]	$N(v,j)$[e]	$G(E^{\#})$[f]	$k(E) \times 10^{11}(1/s)$
153.1	10.7	3.94	162.3	0.8	7	2.5
163.6	23.1	3.05	159.4	0.9	24	8.2
174.0	34.5	2.92	157.5	1.3	54	13.1
184.5	45.7	2.85	156.9	1.6	107	20.6
195.0	57.3	2.78	154.8	1.7	185	31.7
205.4	67.9	2.76	154.2	2.3	300	39.7
215.9	80.0	2.67	152.2	2.7	465	51.0
226.3	91.4	2.63	150.8	3.2	689	64.5
236.8	103.0	2.59	150.1	3.7	984	79.0
247.3	115.0	2.54	148.1	4.5	1375	91.2
257.7	125.9	2.52	147.4	5.2	1860	107.3
268.2	137.7	2.49	146.1	6.2	2478	120.7
278.6	149.4	2.46	145.4	7.3	3238	132.4
289.1	161.2	2.43	143.4	8.1	4169	153.9
299.6	173.5	2.40	140.7	9.7	5290	163.9
310.0	185.8	2.37	138.7	11.1	6622	177.9
320.5	197.4	2.34	137.3	12.6	8141	194.1
330.9	209.2	2.32	136.0	14.4	9982	207.7
341.4	221.3	2.30	134.0	16.5	12120	220.6

a) The total energy available to the system in kJ mol^{-1}. b) The transition-state energy in kJ mol^{-1}. c) The position of bottle-neck in angstrom. d) The classical energy difference between the reactant and the transition state in kJ mol^{-1}. e) The density of states in cm^{-1}. f) The sum of states.

respectively). Values of k_e, k_e', and $G(E_{vr}{}^{+})$ were calculated by using RRKM program from Zhu and Hase.[52] Arrhenius plot for reaction R4 is shown in Fig. 7. As shown in our proposed mechanism, another source for the formation of hydroxyl radical in this system is channel R6, which will be discussed in the next section. We also showed in Fig. 7 the calculated rate constant for channel R6. The dashed line in Fig. 7 shows the rate constant for reaction R4, the formation of OH radicals. The calculated stabilization rate constant R4w (dotted line) in Fig. 7b indicates that the stabilization process for hydrogen

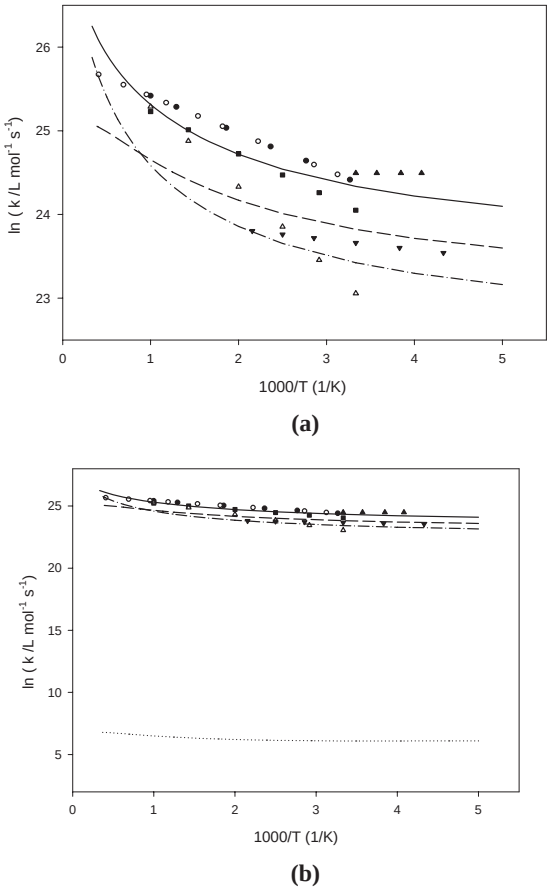

Fig. 7. (a) Arrhenius plot for reactions R4 (dashed line) and R6 (dashed-dot line). Solid line is the sum of dashed line and dashed-dotted line. Symbols from experimental results for the formation of hydroxyl radical: ▲, Ref. 1; ●, Ref. 2; ○, Ref. 4; ■, Ref. 8; ▼, Ref. 9; △, Ref. 7. (b) The overall stabilization rate constants $k_{6w} + k_{4w}$ (dotted line) is compared with the data shown in (a). Stabilization rate constant k_{5w} is shown as dotted line.

peroxide is not an important process at total pressure of 1 atm that means almost all of the formed hydrogen peroxide in this channel dissociates to hydroxyl radicals. Nonlinear least square fitting to the data for k_4 in Fig. 7 gave the following expression for the rate constant of reaction R4: $k_4 = 7.20 \times 10^6 \times T^{1.25} \times \exp(+1.13\,\mathrm{kJ\,mol^{-1}}/RT)\,\mathrm{L\,mol^{-1}\,s^{-1}}$.

Rate Constants for Channels R5 and R6

In our proposed mechanism, energized water oxide (H_2OO^*) in channel R5 is produced over a singlet potential energy surface. Based on Fig. 2 and Table 3, its energy was 160.2, 163.2, and 164.3 kJ mol^{-1} lower than the total energies of the reactants at the CCSD(full), CCSD(T), and G3 levels, respectively, at zero Kelvin. The produced chemically activated water oxide dissociates to water and singlet oxygen atom according to channel R5 or isomerizes to hydrogen peroxide via a [1,2] hydrogen shift as shown in channel R6.[20] Figure 6 shows the potential energy surfaces for reactions R4 and R5 at the CAS/6-311+G(2d,2p) level. No saddle point was found for the entrance or exit channels for the formation of H_2OO^*. Our MC-SCF calculations gave better results regarding to the elimination of the spin contamination for the association or dissociation reactions involved in channels R4 and R5.

To calculate the rate constants for reactions R5 and R6 and the relevant rate constants involved in these two paths, we first searched for the location of the bottlenecks in reaction R5, which are dissociation of water oxide towards $H_2O + O(^1D)$ and $HO_2 + H$. We used the same method to perform microcanonical variational RRKM calculations to locate the position of bottlenecks for this channel as we described in the previous section for channels R4. Tables 8 and 9 show the results of microcanonical variational RRKM calculations for the entrance and exit channels of formation of water oxide towards $HO_2 + H$ (k_{-5a}) or $H_2O + O(^1D)$ (k_{5b}), respectively.

As shown in Fig. 2, isomerization of water oxide to hydrogen peroxide passed over a saddle point with a 25.2 or 15.6 kJ mol^{-1} barrier height at the CCSD(full)/Aug-cc-pVTZ or G3 levels, respectively. A value of 15.5 to 16.3 kJ mol^{-1} at the MP4SDTQ/6-31G* level has been reported for the barrier of this reaction by Bach et al.[20b,20d] As shown in Fig. 2 and listed in Table 3, depending on the level of calculation, the energy of water oxide was 189 to 211 kJ mol^{-1} higher than the energy of hydrogen peroxide. The energy difference between water oxide and hydrogen peroxide has been reported to be 192 to 234 kJ mol^{-1} in the literature (see Refs. 20a to 20j).

The total energy of produced hydrogen peroxide was 193.4, 191.4, and 193.04 kJ mol^{-1} less than water oxide at the CCSD(full), CCSD(T), and G3 levels, respectively. It is expected that this amount of energy release in to the newly formed hydrogen peroxide causes its dissociation into hydroxyl radicals unless it is stabilized via collision. To calculate the rate constants for the formation of $H_2O + O(^1D)$ or $OH(^2\Pi)$ via channels R5 or R6, respectively, we used a method suggested by Dean, which is based on RRKM method.[23] According to this approach, these rate constants can be calculated as

$$k_5 = k_{5a} \sum_{E0}^{\infty} \frac{k_{5b} D' \{G(E^+)\} \exp(-E^+/RT)}{DD' - k_{-6a}(E) k_{6a}(E)}, \quad (7)$$

$$k_{5w} = k_{5a} \sum_{E0}^{\infty} \frac{\omega D' \{G(E^+_{vr})\} \exp(-E^+/RT)}{DD' - k_{6a}(E) k_{-6a}(E)}, \quad (8)$$

$$k_6 = k_{5a} \sum_{E0}^{\infty} \frac{k_{6b}(E) k_{6a} \{G(E^+)\} \exp(-E^+/RT)}{DD' - k_{-6a}(E) k_{6a}(E)}, \quad (9)$$

$$k_{6w} = k_{5a} \sum_{E0}^{\infty} \frac{\omega k_{6a}(E) \{G(E^+)\} \exp(-E^+/RT)}{DD' - k_{-6a}(E) k_{6a}(E)}, \quad (10)$$

where k_{5w} and k_{6w} are the stabilization rate constants for stabilization of H_2OO^* and $HOOH^*$ under collision, respectively, k_5 and k_6 are the overall rate constants for the formation of $H_2O + O(^1D)$ in channel R5 and formation of OH radicals in channel R6, respectively, $D = k_{-5a}(E) + \omega + k_{5b}(E) + k_{6a}(E)$, and $D' = k_{-6a}(E) + \omega + k_{6b}(E)$. Values of $k_{5a}(E)$, $k_{5b}(E)$, $k_{6a}(E)$, $k_{-6a}(E)$, and $k_{6b}(E)$ are calculated from the quotient of the sum of states to the density of states for the relevant step, and $\omega = Z\beta_c[A]$ is the collisional stabilization rate constant. Sum of states and density of states were calculated by using RRKM program from Zhu and Hase.[52] Vibrational frequencies and moments of inertia in Table 5 were used for these calculations. Arrhenius plots for the rate constants k_5

Table 8. Microcanonical Variational RRKM Results for the Unimolecular Dissociation Step R5a

$E(v,j)$[a]	$E^{\#}(v,j)$[b]	$R^{\#}$/Å[c]	E_0[d]	$N(v,j)$[e]	$G(E^{\#})$[f]	$k(E) \times 10^{11}(1/s)$
174.0	17.1	2.29	183.7	1.4	4	0.87
182.4	25.7	2.26	183.4	1.7	10	1.78
190.7	34.1	2.19	182.7	2.0	17	2.52
199.1	42.7	2.18	182.6	2.3	28	3.69
207.5	51.1	2.18	182.6	2.7	46	5.16
215.8	59.5	2.18	182.6	3.2	70	6.52
224.2	67.8	2.18	182.6	3.9	104	7.98
232.6	76.4	2.17	182.5	4.3	152	10.72
240.9	84.7	2.17	182.5	4.7	214	13.70
249.3	93.1	2.17	182.5	5.5	293	16.11
257.7	101.8	2.16	182.5	6.3	396	18.72
266.1	110.2	2.16	182.5	7.1	524	22.24
274.4	118.5	2.16	182.5	7.8	680	26.01
282.8	126.9	2.16	182.5	8.8	872	29.59
291.2	135.5	2.15	182.4	10.1	1109	33.10
299.5	143.9	2.15	182.4	11.3	1388	36.81
307.9	152.2	2.14	182.3	12.6	1721	40.78
316.3	160.6	2.14	182.3	14.1	2118	45.00

a) The total energy available to the system in kJ mol^{-1}. b) The transition-state energy in kJ mol^{-1}. c) The position of bottle-neck in angstrom. d) The classical energy difference between the reactant and the transition state in kJ mol^{-1}. e) The density of states in cm^{-1}. f) The sum of states.

Table 9. Microcanonical Variational RRKM Results for the Unimolecular Dissociation Step R5b

$E(v,j)$[a]	$E^{\#}(v,j)$[b]	$R^{\#}$/Å[c]	E_0[d]	$N(v,j)$[e]	$G(E^{\#})$[f]	$k(E) \times 10^{11}(1/s)$
182.4	25.6	3.77	166.2	1.7	11	2.0
195.0	38.3	3.74	166.0	2.1	25	3.6
207.5	50.8	3.72	165.9	2.7	50	5.6
220.1	63.4	3.69	165.8	3.4	90	8.0
232.6	76.0	3.66	165.7	4.2	152	10.9
245.2	88.6	3.63	165.6	5.1	241	14.2
257.7	100.9	3.62	165.6	6.2	365	17.6
270.3	113.4	3.62	165.6	7.5	538	21.5
282.8	126.0	3.61	165.6	9.0	771	25.7
295.4	138.5	3.61	165.6	10.7	1076	30.1
307.9	151.1	3.61	165.6	12.7	1469	34.7
320.5	163.7	3.60	165.4	14.9	1969	39.5
333.0	176.2	3.60	165.4	17.5	2594	44.4
345.6	188.8	3.60	165.4	20.4	3368	49.5
358.1	201.4	3.59	165.4	23.7	4316	54.6
370.7	213.9	3.59	165.4	27.4	5463	59.9
383.2	226.5	3.59	165.4	31.5	6842	65.2
395.8	239.1	3.58	165.3	36.1	8483	70.5
408.3	251.6	3.58	165.3	41.2	10420	75.9
420.9	264.2	3.58	165.3	46.9	12700	81.2
433.5	276.8	3.57	165.3	60.1	18450	92.0

a) The total energy available to the system in kJ mol^{-1}. b) The transition-state energy in kJ mol^{-1}. c) The position of bottle-neck in angstrom. d) The classical energy difference between the reactant and the transition state in kJ mol^{-1}. e) The density of states in cm^{-1}. f) The sum of states.

for the formation of $H_2O + O(^1D)$ via channel R5 and k_6 for the formation of $OH(^2\Pi)$ radicals via channel R6 are shown in Figs. 8 and 7, respectively.

In Fig. 8a, compared our calculated rate constant k_5 for the formation of $H_2O + O(^1D)$, shown as solid line, with the reported values in the literature. To the best of our knowledge, no comment has been made on the electronic state of produced atomic oxygen in the previous experimental studied on this

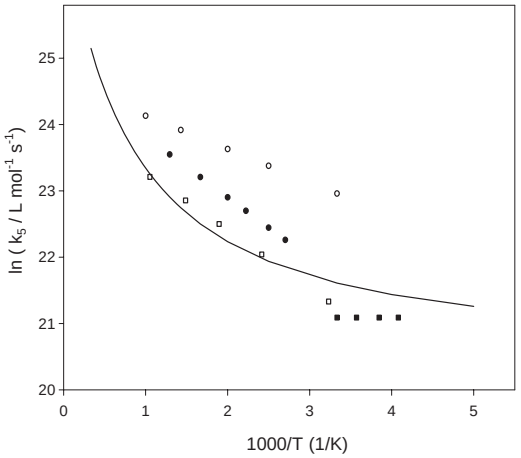

(a)

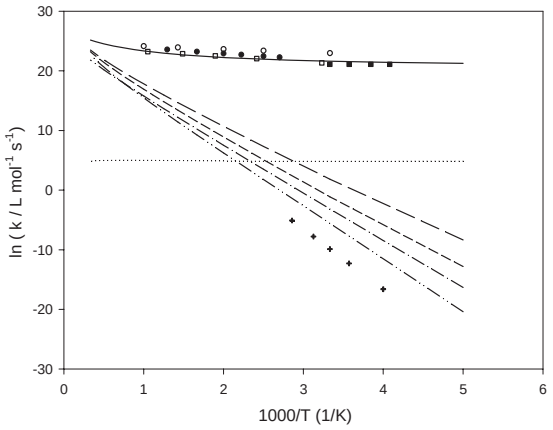

(b)

Fig. 8. (a) Arrhenius plot for reaction R5, solid line from CCSD(full) results, ■ from Ref. 1, □ from Ref. 2, ● Ref. 6, ○ from Ref. 7. (b) The data in Fig. 5 for k_3 is compared with the data in Fig. 8a for k_5. The lines and the symbols in 8b are the same as those explained in Figs. 8a and 5.

system. Also, in Fig. 8b, we compared our calculated rate constant k_3 with the data in Fig. 8a for k_5. As shown in Fig. 8, the major channel for the formation of $H_2O + O$ should be channel R5, of which its value agrees with the experimental results, whereas, reaction R3 is not an important contributor for the formation of $H_2O + O$, see Fig. 7b. The kinetic parameters for k_5 from CCSD(full)/Aug-cc-pVTZ results was calculated as $k_5 = 2.9 \times 10^5 \times T^{1.55} \times \exp(+0.67\,\mathrm{kJ\,mol^{-1}}/RT)\,\mathrm{L\,mol^{-1}\,s^{-1}}$. In Fig. 8b, we also showed the stabilization rate constant for H_2OO^* k_{5w} as a dotted line. Our results shows that stabilization process is not important and almost all of the newly formed water oxides undergo dissociation or isomerization process. The value of stabilization rate constant k_{5w} was calculated to be $1.4 \times 10^2\,\mathrm{L\,mol^{-1}\,s^{-1}}$ and almost independent of the temperature.

The variation of rate constants k_4 (dashed line) and k_6 (dashed-dot line) for the formation of OH($^2\Pi$) as a function of temperature is shown in Fig. 7a. Our results shows that both channels R4 and R6 are important for the formation of hydroxyl radicals. In Fig. 7, we also showed the sum of k_4 and k_6 as solid line, which is compared with reported experimental values of the rate constant for the formation of OH radicals in this system. In Fig. 7b, we have shown that sum of the stabilization processes $k_{4w} + k_{6w}$ (dotted line) is not important, and we expect that most of the newly formed hydrogen peroxides dissociate to hydroxyl radicals. The overall rate constant expression, k(OH) ($=k_4 + k_6$), for the formation of OH radicals via channels R4 and R6 was obtained by nonlinear least squares fitting to the solid line in Fig. 7a as $k(\mathrm{OH}) = 2.2 \times 10^8 \times T^{0.88} \times \exp(+0.27\,\mathrm{kJ\,mol^{-1}}/RT)\,\mathrm{L\,mol^{-1}\,s^{-1}}$. The rate constant expression k_6 by nonlinear least squares fitting to the dashed-dot line in Fig. 7a was found as $k_6 = 5.0 \times 10^9 \times T^{0.35} \times \exp(-1.08\,\mathrm{kJ\,mol^{-1}}/RT)\,\mathrm{L\,mol^{-1}\,s^{-1}}$.

We also calculated the rate of isomerization of water oxide to hydrogen peroxide, reaction R7, by means of RRKM method (Scheme 2). Equation 4 was used to calculate the rate constant k_7 as a function of pressure, and Eq. 11[57] was used to calculate the high-pressure limit for this rate constant.

$$H_2OO \rightarrow HOOH \qquad \text{R7}$$

Scheme 2.

$$k_\infty = \frac{\sigma B_e}{hQ_r}\exp\left(\frac{-E_0}{RT}\right)\int\sum_{J=0}^{\infty}(2J+1)\{G(E^+_{vr})\} \times \exp\left(\frac{-E^+}{RT}\right)dE^+. \qquad (11)$$

To calculate the sum of state, $G(E^+_{vr})$, we used the RRKM program from Zhu and Hase.[52] To calculate the rate constant for reaction R7 according to RRKM method, we used the vibrational term values and moments of inertia listed in Table 5 along with the activation energies of 25.2 and $15.2\,\mathrm{kJ\,mol^{-1}}$ calculated at the CCSD(full) and CCSD(T) levels, respectively. In RRKM calculations, a step size of $\Delta E^+ = 0.4\,\mathrm{kJ\,mol^{-1}}$ up to the $E^+ = 10\,\mathrm{kJ\,mol^{-1}}$ at 200 K, which was increased to a value of $100\,\mathrm{kJ\,mol^{-1}}$ at 3000 K, was used. B_e was assumed to be equal 1. N_2 was chosen as bath gas, and a value of 0.2 was selected for collision efficiency β_c from Ref. 56. We also calculated the tunneling factor according to Ref. 49. Figure 9 shows an Arrhenius plot for reaction R7 from the CCSD(full) and CCSD(T) results including a tunneling correction. The kinetic parameters for this reaction with inclusion of tunneling factor was found to be $k_7 = 8.1 \times 10^{12} \times T^{0.18} \times \exp(-17.5\,\mathrm{kJ\,mol^{-1}}/RT)\,\mathrm{L\,mol^{-1}\,s^{-1}}$ from CCSD(full) results and $k_7 = 1.6 \times 10^{12} \times T^{0.42} \times \exp(-7.9\,\mathrm{kJ\,mol^{-1}}/RT)\,\mathrm{L\,mol^{-1}\,s^{-1}}$ from CCSD(T) results.

Conclusion

Possible reaction paths for $HO_2 + H$ system was studied theoretically. As shown in Table 3, different theoretical methods were used to optimize and calculate the energy of stationary points to assure of our results based on the proposed mechanism. All of the methods in Table 3 showed the same trends for the energies of all stationary points. For instance, we found water oxide as a local minimum on the singlet potential energy surface in all methods of calculations that we used in this study. One difference is that, for reaction R1, no saddle points

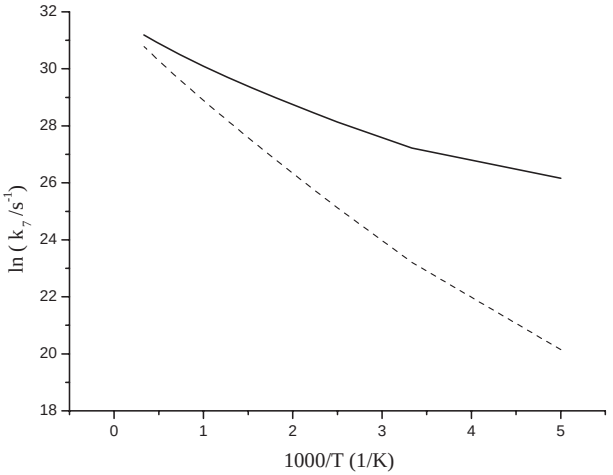

Fig. 9. High-pressure Arrhenius plot for unimolecular isomerization of $H_2OO \rightarrow HOOH$ calculated at the CCSD(T)/Aug-cc-pVTZ level (solid line) and at the CCSD(full)/Aug-cc-pVTZ level (dashed line).

were found using DFT methods and G3 method, whereas a saddle point was found using the other methods. Despite this discrepancy, ab initio methods still indicated that reaction R1 is the major channel for the formation of $H_2 + O_2$.

To the best of our knowledge, the first experimental observation of water oxide (H_2OO) has been reported by Schröder et al.[20f] Our results indicated the presence of such a species, and when we ignored the formation and consumption of this species in this system, it was not possible to get a correct rate constant for the formation of $H_2O + O$ in agreement with the experimental results, as reported by Boutalib et al.[18] and Karkach and Osherov.[19] To the best of our knowledge, there is only one experimental study, in which the electronic state of produced O_2 is considered.[36]

Generalized transition state theory was employed to calculate the rate constants for reactions R1, R2, and R3. To calculate the rate constant for reaction R4 that proceeds trough a chemically activated intermediate HOOH*, a RRKM-TST model from Berman and Lin was used.[22] To calculate the overall rate constants for the formation of $H_2O + O(^1D)$ according to reaction R5 (k_5) and the formation of OH radicals according to reaction R6 (k_6) a method based on RRKM theory that suggested by Dean was used.[23] Microcanonical variational RRKM model was used to locate the position of the bottlenecks of different steps with no saddle point involved in these channels, the entrance and exit channels of H_2OO and HOOH.

Reaction R1 proceeded via a triplet potential energy surface to produce $H_2 + O_2(^3\Sigma_g^-)$, and reaction R2 proceeded via a singlet potential energy surface to produce $H_2 + O_2(^1\Delta)$. As shown in Fig. 4, our calculations indicates that the major path for the formation of $H_2 + O_2$ is reaction R1, of which the barrier height for this reaction was 73.2 kJ mol^{-1} lower than the activation energy for reaction R2 at the CCSD(full)/Aug-cc-pVTZ level.

Reaction R3 proceeded on a triplet surface to produce $H_2O + O(^3P)$, whereas reaction R5 proceeded on a singlet surface to produce $H_2O + O(^1D)$ via the formation of chemically activated intermediate H_2OO^*. As shown in Fig. 8, the major path for the formation of $H_2O + O$ should be reaction R5. Reaction R3 passed through a potential barrier of 79.6 kJ mol^{-1} at CCSD(full)/Aug-cc-pVTZ, whereas reaction R5 proceeded through a chemically activated process.

Both reactions R4 and R6 are responsible for the formation of hydroxyl radicals. Our calculations indicate that both reactions R4 and R6 are important in the formation of OH radicals, as shown in Fig. 7. Our results also show that the major product in this system should be hydroxyl radical, as reported in the previous studies.

According to our calculations for k_{4w}, k_{5w}, and k_{6w}, both energized intermediates H_2OO and HOOH undergo dissociation process much faster than stabilization process. Therefore, we do not expect that these two species are products in this system, especially at high temperatures. These results are in agreement with the experimental reports in the literature, that is none of these species have been reported as the possible product in this system.

References

1 R. Atkinson, D. L. Baulch, R. A. Cox, R. F. Hampson, Jr., J. A. Kerr, M. J. Rossi, J. Troe, *J. Phys. Chem. Ref. Data* **1997**, *26*, 1329.

2 D. L. Baulch, C. J. Cobos, R. A. Cox, C. Esser, P. Frank, Th. Just, J. A. Kerr, M. J. Pilling, J. Troe, R. W. Walker, J. Warnatz, *J. Phys. Chem. Ref. Data* **1992**, *21*, 411.

3 Y. Hidaka, T. Taniguchi, H. Tanaka, T. Kamesawa, K. Inami, H. Kawano, *Combust. Flame* **1993**, *92*, 365.

4 W. Tsang, R. F. Hampson, *J. Phys. Chem. Ref. Data* **1986**, *15*, 1087.

5 U. C. Sridharan, L. X. Qiu, F. Kaufman, *J. Phys. Chem.* **1982**, *86*, 4569.

6 R. R. Baldwin, R. W. Walker, *J. Chem. Soc., Faraday Trans. 1* **1979**, *75*, 140.

7 A. C. Lloyd, *Int. J. Chem. Kinet.* **1974**, *6*, 169.

8 J. Warnatz, in *Combustion Chemistry*, ed. by W. C. Gardiner, Jr., Springer-Verlag, NY, **1984**, p. 197.

9 G. L. Pratt, S. W. Wood, *J. Chem. Soc., Faraday Trans. 1* **1983**, *79*, 2597.

10 R. Shaw, *Int. J. Chem. Kinet.* **1977**, *9*, 929.

11 G. Dixon-Lewis, A. Williams, *Nature* **1962**, *196*, 1309.

12 A. A. Westenberg, N. DeHaas, *J. Phys. Chem.* **1972**, *76*, 1586.

13 R. R. Baldwin, M. E. Fuller, J. S. Hillman, D. Jackson, R. W. Walker, *J. Chem. Soc., Faraday Trans. 1* **1974**, *70*, 635.

14 W. Hack, A. W. Preuss, H. G. Wagner, K. Hoyermann, *Ber. Bunsen-Ges. Phys. Chem.* **1979**, *83*, 212.

15 B. A. Thrush, J. P. T. Wilkinson, *Chem. Phys. Lett.* **1981**, *84*, 17.

16 U. C. Sridharan, L. X. Qiu, F. Kaufman, *J. Phys. Chem.* **1982**, *86*, 4569.

17 L. F. Keyser, *J. Phys. Chem.* **1986**, *90*, 2994.

18 A. Boutalib, H. Cardy, C. Chevaldonnet, M. Chaillet, *Chem. Phys.* **1986**, *110*, 295.

19 S. P. Karkach, V. I. Osherov, *J. Chem. Phys.* **1999**, *110*, 11918.

20 a) R. D. Bach, A. L. Owensby, C. Gonzalez, H. B. Schlegel, *J. Am. Chem. Soc.* **1991**, *113*, 2338. b) R. D. Bach, A. L. Owensby, C. Gonzalez, H. B. Schlegel, J. J. W. McDouall, *J. Am. Chem. Soc.* **1991**, *113*, 6001. c) R. D. Bach, H. B. Schlegel,

J. L. Andres, C. Sosa, *J. Am. Chem. Soc.* **1994**, *116*, 3475. d) R. D. Bach, M.-D. Su, *J. Am. Chem. Soc.* **1994**, *116*, 10103. e) J.-W. Chu, B. L. Trout, *J. Am. Chem. Soc.* **2004**, *126*, 900. f) D. Schröder, C. A. Schalley, N. Goldberg, J. Hrusak, H. Schwarz, *Chem. Eur. J.* **1996**, *2*, 1235. g) C. Meredith, T. P. Hamilton, H. F. Schaefer, III, *J. Phys. Chem.* **1992**, *96*, 9250. h) H. H. Huang, Y. Xie, H. F. Schaefer, III, *J. Phys. Chem.* **1996**, *100*, 6076. i) R. Sayós, C. Oliva, M. Gonzalez, *J. Chem. Phys.* **2000**, *113*, 6736. j) M. Filatov, W. Reekien, S. D. Peyerimhoff, S. Shaik, *J. Phys. Chem. A* **2000**, *104*, 12014.

21 D. W. Toohey, J. G. Anderson, *J. Phys. Chem.* **1989**, *93*, 1049.

22 M. R. Berman, M. C. Lin, *J. Phys. Chem.* **1983**, *87*, 3933.

23 A. M. Dean, *J. Phys. Chem.* **1985**, *89*, 4600.

24 M. J. Frisch, G. W. Trucks, H. B. Schlegel, G. E. Scuseria, M. A. Robb, J. R. Cheeseman, J. A. Montgomery, Jr., T. Vreven, K. N. Kudin, J. C. Burant, J. M. Millam, S. S. Iyengar, J. Tomasi, V. Barone, B. Mennucci, M. Cossi, G. Scalmani, N. Rega, G. A. Petersson, H. Nakatsuji, M. Hada, M. Ehara, K. Toyota, R. Fukuda, J. Hasegawa, M. Ishida, T. Nakajima, Y. Honda, O. Kitao, H. Nakai, M. Klene, X. Li, J. E. Knox, H. P. Hratchian, J. B. Cross, C. Adamo, J. Jaramillo, R. Gomperts, R. E. Stratmann, O. Yazyev, A. J. Austin, R. Cammi, C. Pomelli, J. W. Ochterski, P. Y. Ayala, K. Morokuma, G. A. Voth, P. Salvador, J. J. Dannenberg, V. G. Zakrzewski, S. Dapprich, A. D. Daniels, M. C. Strain, O. Farkas, D. K. Malick, A. D. Rabuck, K. Raghavachari, J. B. Foresman, J. V. Ortiz, Q. Cui, A. G. Baboul, S. Clifford, J. Cioslowski, B. B. Stefanov, G. Liu, A. Liashenko, P. Piskorz, I. Komaromi, R. L. Martin, D. J. Fox, T. Keith, M. A. Al-Laham, C. Y. Peng, A. Nanayakkara, M. Challacombe, P. M. W. Gill, B. Johnson, W. Chen, M. W. Wong, C. Gonzalez, J. A. Pople, *Gaussian 03, Revision B.01*, Gaussian, Inc., Pittsburgh PA, **2003**.

25 M. J. Frisch, M. Head-Gordon, J. M. Pople, *Chem. Phys. Lett.* **1990**, *166*, 281.

26 A. D. Becke, *J. Chem. Phys.* **1993**, *98*, 5648.

27 J. K. Kang, C. B. Musgrave, *J. Chem. Phys.* **2001**, *115*, 11040.

28 B. O. Roos, *Advances in Chemical Physics*, **1987**, Vol. 69, p. 399.

29 G. E. Scuseria, H. F. Schaefer, III, *J. Chem. Phys.* **1989**, *90*, 3700.

30 L. A. Curtiss, K. Raghavachari, P. C. Redfern, V. Rassolov, J. A. Pople, *J. Chem. Phys.* **1998**, *109*, 7764.

31 R. A. Kendall, T. H. Dunning, Jr., R. J. Harrison, *J. Chem. Phys.* **1992**, *96*, 6796.

32 C. Gonzalez, H. B. Schlegel, *J. Phys. Chem.* **1990**, *94*, 5523.

33 L. V. Gurvich, I. V. Veyts, C. B. Alcock, *Thermodynamics Properties of Individual Substances*, 4th ed., Hemisphere Pub. Co., New York, **1989**.

34 J. D. Cox, D. D. Wagman, V. A. Medvedev, *CODATA Key Values for Thermodynamics*, Hemisphere Pub. Co., New York, **1989**.

35 B. Ruscic, A. F. Wagner, L. B. Harding, R. L. Asher, D. Feller, P. A. Dixon, K. A. Peterson, Y. Song, X. Qian, C. Y. Ng, J. Liu, W. Chen, D. W. Schwenke, *J. Phys. Chem. A* **2002**, *106*, 2727.

36 N. Washida, H. Akimoto, M. Okuda, *J. Phys. Chem.* **1978**, *82*, 18.

37 M. E. Jacox, *J. Phys. Chem. Ref. Data* Monograph 3, **1994**.

38 A. Charo, F. De Lucia, *J. Mol. Spectrosc.* **1982**, *94*, 426.

39 T. Shimanouchi, *Tables of Molecular Vibrational Frequencies*, Consolidated Vol. 1, NSRDS NBS-39, **1972**, Consolidated Vol. 1.

40 G. Herzberg, *Electronic Spectra and Electronic Structure of Polyatomic Molecules*, Van Nostrand, New York, **1966**.

41 R. L. Redington, W. B. Olson, P. C. Cross, *J. Chem. Phys.* **1962**, *36*, 1331.

42 K. P. Huber, G. Herzberg, *Molecular Spectra and Molecular Structure. IV. Constants of Diatomic Molecules*, Van Nostrand Reinhold Co., **1979**.

43 D. G. Truhlar, A. D. Isaacson, B. C. Garrett, in *Theory of Chemical Reaction Dynamics*, ed. by M. Baer, CRC Press, Boca Raton, FL, **1985**.

44 E. P. Wigner, *Z. Phys. Chem. B* **1932**, *19*, 203.

45 M. J. Stern, R. E. Weston, Jr., *J. Chem. Phys.* **1974**, *60*, 2803; **1974**, *60*, 2808; **1974**, *60*, 2815.

46 C. Eckart, *Phys. Rev.* **1930**, *35*, 1303.

47 I. Shavitt, *J. Chem. Phys.* **1959**, *31*, 1359.

48 M. Bowdridge, H. Furue, P. D. Pacey, *J. Phys. Chem.* **1996**, *100*, 1676.

49 R. L. Brown, *J. Res. Natl. Bur. Stand. (U.S.)* **1981**, *86*, 357.

50 J. V. Michael, J. W. Sutherland, L. B. Harding, A. F. Wagner, *Proc. Combust. Inst.* **2000**, *28*, 1471.

51 L. B. Harding, *J. Phys. Chem.* **1989**, *93*, 8004; **1991**, *95*, 8653; Ch. Kappel, K. Luther, J. Troe, *Phys. Chem. Chem. Phys.* **2002**, *4*, 4392.

52 L. Zhu, W. L. Hase, *QCPE Program 644; Quantum Chemistry Program Exchange*, Indiana University, Bloomington, IN, **1993**.

53 K. A. Holbrook, M. J. Pilling, S. H. Robertson, *Unimolecular Reactions*, 2nd ed., John Wiley & Sons Ltd. Chichester, England, **1996**.

54 L. Zhu, W. Chen, W. L. Hase, *J. Phys. Chem.* **1993**, *97*, 311.

55 D. C. Tardy, B. S. Rabinovitch, G. Z. Whitten, *J. Chem. Phys.* **1968**, *48*, 1427.

56 L. E. B. Börjesson, S. Nordholm, *J. Phys. Chem.* **1995**, *99*, 938.

57 D. M. Wardlaw, R. A. Marcus, *J. Phys. Chem.* **1986**, *90*, 5383.